Endothelial cell-initiated extravasation of cancer cells visualized in zebrafish

The extravasation of cancer cells, a key step for distant metastasis, is thought to be initiated by disruption of the endothelial barrier by malignant cancer cells. An endothelial covering-type extravasation of cancer cells in addition to conventional cancer cell invasion-type extravasation was dynamically visualized in a zebrafish hematogenous metastasis model. The inhibition of VEGF-signaling impaired the invasion-type extravasation via inhibition of cancer cell polarization and motility regulated by an intracellular signaling. Paradoxically, the inhibition of VEGF-signaling showed the promotion, rather than the inhibition, of the endothelial covering-type extravasation of cancer cells, with structural changes in the endothelial walls. These findings may be a clue to the full understanding of the metastatic process as well as the metastatic acceleration by antiangiogenic reagents observed in preclinical studies.

1 **Endothelial cell-initiated extravasation of cancer cells visualized in zebrafish**

2

3 **Masamitsu Kanada[1,a], Jinyan Zhang[1], Libo Yan[1], Takashi Sakurai[2] and Susumu**

4 **Terakawa[1,b,*]**

5

6 [1]Medical Photonics Research Center, Hamamatsu University School of Medicine, 1-20-1

7 Handayama, Higashi-ku, Hamamatsu, 431-3192, Japan

8 [2]Electronics-inspired Interdiciplinary Research Institute, Toyohashi University of Technology, 1-1

9 Hibarigaoka, Tempaku, Toyohashi, 441-8580, Japan

10

11 [*]To whom correspondence may be addressed. E-mail: terakawa@sz.tokoha-u.ac.jp

12 [a] Present address: Department of Pediatrics, Stanford University School of Medicine, Clark

13 Center E150, 318 Campus Drive, Stanford, CA 94305, USA

14 [b] Present address: Department of Health Science, Tokoha University, 1-22-1 Sena, Aoi-ku,

15 Shizuoka, 420-0911, Japan

16

17

18   **Abstract**

19   The extravasation of cancer cells, a key step for distant metastasis, is thought to be initiated by

20   disruption of the endothelial barrier by malignant cancer cells. An endothelial covering-type

21   extravasation of cancer cells in addition to conventional cancer cell invasion-type extravasation

22   was dynamically visualized in a zebrafish hematogenous metastasis model. The inhibition of

23   VEGF-signaling impaired the invasion-type extravasation via inhibition of cancer cell

24   polarization and motility regulated by an intracellular signaling. Paradoxically, the inhibition of

25   VEGF-signaling showed the promotion, rather than the inhibition, of the endothelial covering-

26   type extravasation of cancer cells, with structural changes in the endothelial walls. These findings

27   may be a clue to the full understanding of the metastatic process as well as the metastatic

28   acceleration by antiangiogenic reagents observed in preclinical studies.

29

30

Introduction

Metastasis is the primary factor associated with the death of cancer patients. There is no therapeutic agent available to prevent this pathological step [1]. Metastatic progression proceeds by multiple steps: first, the development of vasculature inside a primary nest of tumor, intravasation of tumor cells into the newly developed leaky vasculature, survival of the cells under the stress in the systemic circulation, extravasation of the cells from the circulation, and finally proliferation at a secondary site in a distant tissue [2]. These steps have been verified by studies of cancer cells or endothelial cells under *in vitro* culture conditions, or by examining preparations of fixed tissue specimens. Although histological or biochemical techniques may provide important information, such information is only validated at a certain point of time and thus compromises the interpretation on the dynamic aspects of metastasis. One of the difficulties in observing the behavior of cancer cells *in vivo* in mice by conventional high-resolution imaging techniques is the low transparency of the tissue. Advanced techniques for intravital observations, such as two-photon microscopies, imaging chamber recording, fiber-optic fluorescence microendoscopies, have gradually enabled the visualization of the dynamic environmental changes accompanying tumor development at a cellular level [3-5]. However, no study has so far clearly shown the whole process of metastasis in mammalian tumor models at the cellular level.

A novel imaging technique was developed to overcome these difficulties in observing the dynamic process of cancer cell metastasis *in vivo*, taking advantage of the high transparency of zebrafish [6-8]. The zebrafish is an ideal vertebrate model for imaging, not only because of its optical transparency but also because a comparison of the zebrafish genome with human's revealed a remarkable conservation in the sequence of genes associated with the cell cycle, tumor suppression, proto-oncogenes, angiogenic factors, and extracellular matrix proteins [9-11]. Highly metastatic cancer cells are often trapped in the capillaries and efficiently extravasated in

55   the zebrafish, and an overexpression of the pro-metastatic gene "Twist" in cancer cells

56   dramatically promotes their intravascular migration and extravasation [7].

57   The present study extended the zebrafish hematogenous metastasis model, and thereby made

58   it possible to study the extravasation of human cancer cells especially after forming severe

59   emboli in the arterioles of zebrafish. The results obtained using a long-time fluorescence time-

60   lapse recording system demonstrate that human cancer cells extravasate according to the manner

61   generally accepted as an active invasion of a cancer cells. An extraordinary event was that a mass

62   of cancer cells underwent embolus formation and then also extravasated via a covering with a

63   layer of endothelial cells even in the absence of active invasion of the cancer cells. An electron

64   microscopic study of a mouse lung metastasis model revealed similar cancer cell extravasation

65   many years ago [12]. A dynamic observation method demonstrated that the covering by

66   endothelial cells is the major event in cancer cell extravasation. Furthermore, the live observation

67   system confirmed that VEGF was associated with this manner of extravasation. Paradoxically,

68   the treatment with an anti-angiogenic inhibitor shows the promotion, rather than the prevention,

69   of the endothelial covering-type extravasation.

70

Results

Extravasation of Embolus-forming Human Cancer Cells

This study first examined the potential for the extravasation of human cervical cancer cells (HeLa). RFP-expressing HeLa (RFP-HeLa) cells were microinjected into the circulation, following the protocol previously reported [7]. Unlike the previous study reporting that injected cancer cells are arrested in the thinner intersegmental vessels [7], RFP-HeLa cells formed severe emboli mostly in the thicker caudal artery immediately after injecting into the circulation. The clusters of cancer cells in the emboli extravasated and adhered to the tissue outside the blood vessels after 17 - 20 h (**Figure 1A**). The spatial distribution of the adhering-cancer cells and blood vessel-forming endothelial cells was evaluated using a confocal microscope 1 day after the cancer cell injection to confirm that embolus-forming cancer cells actually extravasated and developed adhesion to the tissue outside the blood vessels. The optically sliced images clearly showed that endothelial tube structures were devoid of the mass of cancer cells, and all of the RFP-HeLa cells adhered to the tissue outside the blood vessels (**Figure 1B**). Therefore, RFP-HeLa cells, which formed severe emboli in thicker caudal artery of zebrafish, have the ability to efficiently extravasate and adhere to the tissues surrounding the blood vessels.

Two Processes of Extravasation in Human Cancer Cells

The process of extravasation by the RFP-HeLa cells was observed using a long-time dual color time-lapse recording system to study mechanisms of extravasation of human cancer cells. The embolus-forming RFP-HeLa cells and endothelial cells could be observed for more than 11 h, which was long enough for these cells to exhibit slow behaviors. There were two distinctive processes of extravasation observed in RFP-HeLa cells (**Figure 2A**). Some of the cancer cells actively invaded into the vessel wall and penetrated the wall in the process broadly accepted as

95   the process of extravasation [7,13] (referred to as cancer cell invasion; **Figure 2A, left; Movie**

96   **S1**). In contrast, other masses of cancer cells seemed to be quiescent. These cells did not invade

97   the endothelial cell layer. Instead, a new leaf of endothelial cells appeared and extended over the

98   embolus-forming cells. The endothelial cells eventually covered the cancer cells on the vessel

99   wall. Simultaneously, the original layer of endothelial cells gradually disappeared and the cluster

100   of cancer cells spread to the tissue outside of the blood vessels (referred to as endothelial

101   covering; **Figure 2A, right; Movie S2**). Intriguingly, 9 out of 17 extravasations were carried out

102   in the absence of cancer cells' active invasion, while 5 were clearly accompanied by invasion of

103   cancer cells. In the remaining 3 extravasations, embolus-forming cancer cells showed invasion

104   and surrounding endothelial cells also newly extended over the cancer cells (**Figure 2B**). The

105   spatial distribution of embolus-forming cancer cells and newly spreading endothelial cells was

106   further analyzed using 3D confocal microscopic images (47 slices, step size: 1 μm) that were

107   taken at 10 h postadministration. Side views of the stack image and 3D reconstructed image

108   clearly showed that some endothelial cells were extending over the cancer cells or penetrating

109   into the cluster of cancer cells (**Figure 2C; Movie S3**). These results suggest that efficient

110   activation of endothelial cells by cancer cells is also important for extravasation, in addition to

111   high motility of cancer cells, which has been regarded as one of the most crucial factors

112   associated with malignancy.

113   Normal proliferating fibroblast 3T3 cells (NIH, USA) showed neither the invasion type nor the

114   endothelial covering type extravasation in this model. Six clusters of these cells were in the

115   vessels of 6 different individual fish for more than 11 h. All of them formed severe emboli similar

116   to those of cancer cells, but showed neither the development of strong adhesions to the vascular

117   walls nor the process of extravasation mentioned above. This suggests a difference to exist in the

118   expression of adhesion molecules between tumorigenic cells and normal cells, and adhesion to

119 the endothelial walls is a key to induce extravasation for the circulating cancer cells after forming

120 an embolus in the blood vessels.

121

122 **Effects of VEGF Depletion on Cancer Cell Properties and Extravasation**

123 Malignant tumors actively induce new blood vessels from surrounding tissues by secreting

124 vascular endothelial growth factor (VEGF) to receive nutrients and oxygen. In addition, cancer

125 cells may intravasate through this newly-formed leaky vasculature, leading to the metastasis in

126 remote places [14,15]. Hence we examined the effects of depletion of VEGF expressed in RFP-

127 HeLa cells to study the role of VEGF in tumor cell extravasation. The cells were transfected with

128 siRNA prior to their injection into the vessel of the fish. The efficient depletion of VEGF was

129 confirmed by real-time quantitative PCR (RT-qPCR). All the 3 family members of VEGFA,

130 which are secreted by cancer cells, have the same target sequence so that all the VEGFA (referred

131 to as VEGF, here) were depleted in the cancer cells. Expression of VEGF was depleted to 29 ±

132 6% in comparison to the control obtained by using nonsense siRNA-treated cells (**Figure 3A**).

133 The effect of VEGF depletion on the cancer cell itself was then evaluated morphologically *in*

134 *vitro*. The VEGF-depleted cells tended to aggregate with their motility decreased uniformly. They

135 were flattened and their adhering surface became very large (**Figure 3B; Movie S5**). Quantitative

136 evaluation indicated that cell motility was reduced to 36.0 ± 7.7% in comparison to the control

137 obtained by using nonsense siRNA-treated cells as reported previously [16] (**Figure 3C**).

138 Vinculin, a focal adhesion protein, was immunostained in nonsense siRNA-treated and VEGF

139 siRNA-treated RFP-HeLa cells to examine the effects of VEGF depletion on the adhesive

140 property of cancer cells. Focal adhesions were uniformly formed at the cell periphery in VEGF

141 depleted-cells, but only locally in control siRNA-treated cells so as to form a highly polarized

142 shape (**Figure 3D**). These results suggest that VEGF is involved not only in the activation of

143 endothelial cells, but also in the migration of cancer cells via cell polarization.

144   VEGF may regulate the cell motility and cell morphology either directly by an intracellular

145   signaling or indirectly via an autocrine pathway. To study these possible mechanisms, VEGF-

146   depleted cells were cultured in a medium taken from the supernatant of normal RFP-HeLa cell

147   culture (48 h) which would contain VEGF secreted from the normal RFP-HeLa cells to

148   distinguish whether the effect of VEGF was mediated by an intracellular signaling or by an

149   autocrine pathway. The culture medium was replaced with the RFP-HeLa-cultured medium 24 h

150   after the transfection of siRNA against VEGF, and the VEGF-depleted cells were cultured for

151   another 24 h, but the cells did not show any morphological recovery in comparison to the VEGF-

152   depleted cells cultured in a fresh medium (**Figure S1**). Therefore, the effects of VEGF on cell

153   morphology and motility are exerted by the VEGF-involving intracellular signaling.

154   We next examined the effects of VEGF depletion on extravasation *in vivo*. Like the normal

155   RFP-HeLa cells, the VEGF-depleted cells immediately formed emboli after being injected into

156   blood vessels, and then the endothelial cells migrated over the embolus-forming cancer cells,

157   although the process was markedly delayed (**Figure 3E**). Strikingly, the process of cancer cell

158   invasion through the endothelial cells was completely suppressed during the 11-h observation

159   period (**Figure 3E and 3F; Movie S6**). Despite the severe inhibition of cancer cell invasion, most

160   of the VEGF-depleted cells extravasated and adhered to the tissue outside the blood vessels as

161   normal RFP-HeLa cells did within 60 h after transfection at the latest, thus suggesting that the

162   clinically adopted anti-angiogenic strategy of VEGF targeting is insufficient for the prevention of

163   metastasis.

164

165 **Effects of a Multi-targeted Anti-angiogenic Kinase Inhibitor on Cancer Cell**

166 **Properties and Extravasation**

167 VEGF depletion in RFP-HeLa cells only delayed the endothelial covering-type extravasation,

168 while completely inhibiting the cancer cell invasion-type extravasation. Therefore we anticipated

169   that a potent inhibitor of tumor angiogenesis via VEGF signaling could completely inhibit both

170   types of extravasation. Sunitinib (Sutent®, Pfizer Inc.), which effectively suppresses

171   angiogenesis by inhibiting signaling from the receptors for VEGF and for platelet derived growth

172   factor (PDGF) [17,18], was orally administered to the zebrafish larvae. The thinner

173   intersegmental vessels were severely deteriorated by the overnight treatment with sunitinib

174   (**Figure 4A**). However, the thicker blood vessels were not affected morphologically, suggesting

175   that the effect of sunitinib is limited to the newly-formed vulnerable vessels. Endothelial cells in

176   the mature vasculature are independent of VEGF signaling for survival [19,20]. Sunitinib inhibits

177   the VEGF receptor, so the treatment of cells with sunitinib should affect the cancer cells like

178   VEGF depletion. As expected, the cells examined *in vitro* adhered to an obviously larger area of

179   the substrate, became less motile, and tended to aggregate in the presence of sunitinib, as the

180   VEGF-depleted cells did (**Figure S2A**). In addition, the sunitinib treatment reduced the cell

181   motility by $35.0 \pm 5.5\%$ (**Figure S2B**). Focal adhesions were uniformly formed at the cell

182   periphery in sunitinib-treated cells, as in VEGF-depleted cells (**Figure S2C**).

183   The effect of sunitinib on extravasation was examined *in vivo*. Sunitinib treatment completely

184   suppressed the process of cancer cell invasion-type extravasation as expected. Unexpectedly, the

185   incidence of endothelial covering-type extravasation of RFP-HeLa cells was not affected by

186   treatment with sunitinib, although the process was markedly delayed, similar to the extravasation

187   of VEGF-depleted cells (**Figure 4B; Movie S7**). The area of cancer cells that were covered by

188   the endothelial cells in the presence of sunitinib was markedly larger than that in normal or

189   VEGF-depleted RFP-HeLa cells in most events of extravasation, and the blood vessel walls

190   concurrently, but slowly, moved toward the embolus-forming RFP-HeLa cells (**Figure 4B;**

191   **Movie S7**). Therefore, the sum of the area of extravasated cancer cells was calculated from 7

192   movies that were recorded in RFP-HeLa cells with and without sunitinib treatments to

193   quantitatively compare the whole volume of cancer cells extravasated, (**Figure S2D**). Although

194 the incidence of endothelial covering-type extravasation in the presence of sunitinib (9 incidences

195 in 7 larvae) was the same as that observed without treatment of sunitinib (**Figure 2B and 4C**),

196 sunitinib treatment increased the total volume of extravasated cancer cells to 153% of the volume

197 of extravasated cells without sunitinib treatment during 11-h observation period (**Figure 4D**).

198 These results suggest that the anti-angiogenic inhibitor sunitinib can completely suppress the

199 cancer cell invasion-type extravasation without having strong effects on the incidence of

200 endothelial covering-type extravasation. Paradoxically, the total volume of the extravasated

201 cancer cells increased in the presence of sunitinib, thus suggesting that sunitinib accelerates the

202 process independently of the VEGF signaling. Moreover, the endothelial cells apparently

203 activated by sunitinib were studied morphologically using a scanning electron microscope. Many

204 protrusions were observed on the luminal face of endothelial walls of arteries in zebrafish, and

205 interestingly, many small holes were found in some regions on the endothelial wall (**Figure 4F**).

206 These holes are reminiscent of fenestrated endothelial walls in tumor vasculature or normal

207 microvasculature of mice [21-23]. Sunitinib-treated zebrafish larvae showed no hole on the

208 endothelial walls of arteries with fewer protrusions (**Figure 4H**), and also showed prominently

209 thicker endothelial walls (**Figure 4G**).

210

Discussion

Most reports addressing tumor metastasis present evidence supporting the assumption that extravasation and intravasation are initiated by disruption of endothelial barrier by malignant cancer cells via VEGF secretion and invasion [13]. The present study observed a new process, refreshing the conventional understanding of the mechanism of metastasis. A unique hematogenous metastasis model in the transparent zebrafish was used to observe the extravasation of human cancer cells after embolus formation at a cellular level. This approach revealed that extravasation is provoked by a mass of cancer cells, and not by a single cell individually like the invasion of immune cells [24]. The results confirmed that the extravasation is initiated by extension of new leaf of endothelial cells covering the mass of tumor cells in the capillary [12]. The invasion of cancer cells through the endothelium did occur as in the widely accepted model of cancer metastasis. The study demonstrated that VEGF produced by the tumor cells is involved in regulation of their migration by affecting the cell adhesion and polarization via an intracellular signaling, and VEGF-depletion completely suppressed the cancer cell invasion-type extravasation. On the other hand, the endothelial covering-type extravasation was not inhibited but simply delayed by VEGF depletion, suggesting that the process is partially dependent on VEGF and redundant pathways could compensate to complete the extravasation. Sunitinib, an anti-angiogenic inhibitor, suppresses the migration and proliferation of endothelial cells and the migration of the cancer cells simultaneously during the extravasation. Surprisingly, sunitinib treatment had no significant effect on the process of endothelial covering in the current metastasis model system, although it obviously inhibited the new formation of intersegmental vasculature in the zebrafish. Furthermore, ultrastructural observations of the luminal face of an artery in zebrafish showed that the sunitinib treatment eliminated the fenestration-like holes on the endothelium and induced thicker vascular walls. These findings suggest that sunitinib induces

235 vascular maturation independent of VEGF, while deteriorates newly-formed vasculature. VEGF-
236 independent vascular remodeling could be a key regulatory mechanism underlying the
237 extravasation of cancer cells.

238 The current findings also suggest that cancer cells have the potential to extravasate not only in
239 capillary vessels but also in mature blood vessels by forming clusters inducing vascular
240 remodeling. It is worth noting that extravasation of cancer cells as clusters is likely to increase the
241 chance of cancer cells to survive in the tissue outside the vasculature via secretion of trophic
242 factors for their growth or signal molecules for the immune tolerance in comparison to the
243 extravasation of a single cell.

244 Surprisingly, a VEGF-targeted inhibitor promoted the process of endothelial covering over
245 embolic cancer cells independently of VEGF, rather than inhibiting it. Similar evidence has been
246 presented in some preclinical studies, showing that VEGF-targeted inhibition promotes tumor
247 invasiveness and metastasis [25,26]. The explanation for these apparently paradoxical effects
248 were observed in these studies is still controversial [27]. Pàez-Ribes *et al*. (2009) demonstrated
249 that it appears to be an adaptive/evasive response by the tumor cells triggered by a disruption of
250 the tumor vasculature [26]. One plausible mechanism to trigger the adaptation of the tumor cells
251 is tumor hypoxia [28]. The anti-angiogenic treatment disrupts tumor vasculature in the initial
252 phase, but a mechanism of evasive resistance to the anti-angiogenic treatment is then switched on
253 to enable revascularization via alternative pro-angiogenic signals that increase local invasiveness,
254 and/or enhance distant metastasis. Hypoxia is an effective driving force for the evasive resistance
255 of tumors through stabilization of hypoxia inducible factor-1 (HIF-1) [29]. Another study also
256 reported that sunitinib, a VEGF-targeted inhibitor, promotes tumor metastasis in a preclinical
257 model. Immunocompromised mice were pretreated or treated with sunitinib immediately after
258 intravenous inoculation with tumor cells [25]. Intriguingly, the anti-angiogenic treatment
259 increased the formation of metastatic foci, and shortened the overall survival time of the mice.

260 This acceleration of metastasis cannot be explained only by the mechanism of aforementioned

261 hypoxia-related effects on primary tumors. Therefore, the anti-angiogenic VEGF-targeted

262 inhibition may change the nature of vasculature increasing the probability of cancer cell lodging

263 and extravasation. The VEGF-disruption in mice can lead to a vessel disintegration, and render

264 the endothelium prothrombotic [20], which probably increases the number of places where cancer

265 cells lodge.

266   Many investigations reveal that there are multiple types of endothelial cells that have distinct

267 molecular signatures [23,30]. Among these studies, Mazzone *et al*. (2009) reported that a

268 heterozygous deficiency of the oxygen-sensing prolyl hydroxylase domain protein2 (PHD2)

269 reverts the abnormal tumor vasculature formed in the tumor-burdened mice to the mature and

270 stable one, containing an orderly formed tight monolayer of endothelial cell known as "phalanx

271 cells" [23]. The sunitinib-treated endothelial cells in our model are reminiscent of the "phalanx

272 cells" in that the vascular walls, observed in the sunitinib resistant monolayer endothelial cells in

273 the current study. The current findings provide a novel model to explain the complicated

274 phenomena related to the anti-angiogenic strategies against a variety of cancers. The VEGF

275 dependency and fenestration reveals that 2 types of endothelial cell populations are present in the

276 vasculature: one is the VEGF dependent and fenestrated-type, which are defined as active

277 endothelial cells that form new vasculature, and the other is the VEGF independent and

278 unfenestrated-type, which are quiescent endothelial cells that form a mature vasculature. The

279 application of anti-angiogenic inhibitors causes the new vasculature to deteriorate by apoptosis of

280 the active endothelial cells or by vascular maturation. In turn, the quiescent endothelial cells

281 could be reactivated for reconstruction of vessels independently of VEGF in order to maintain the

282 homeostasis of the vasculature (**Figure 5**). Some clinical or preclinical studies show that pro-

283 angiogenic factors other than VEGF are induced by the anti-angiogenic treatment [31-33]. This

284 evidence supports the current model that a disruption of neovascular endothelium by anti-

285 angiogenic drugs promotes endothelial covering-type extravasation via reactivation of quiescent

286 endothelial cells.

287   Anti-VEGF drugs such as the monoclonal anti-VEGF antibody bevacizumab [34,35] and the

288 multi-targeted receptor tyrosine kinase inhibitors sunitinib [36,37] and sorafenib [38,39] prolong

289 the life of some cancer patients, but the clinical benefits of the treatment are relatively modest

290 and usually prolong the overall survival of cancer patients by only months, without offering an

291 enduring cure [40,41], and in some cases it may shorten the survival by facilitating the tumor

292 invasiveness and metastasis. Although the mechanisms of the resistance to anti-angiogenic

293 treatments and acceleration of metastasis are still under investigation, intrinsic tumor resistance

294 or acquired resistance are proposed as possible mechanisms.

295   It is important to understand the complicated mechanism of vascular homeostasis during the

296 anti-angiogenic treatment of such tumors, because the effects of anti-angiogenic drugs on the

297 response of endothelial cells and on the intravasation and extravasation play a key role in each

298 step of metastasis.

299

Materials and Methods

301 **Cell lines**

302 DsRed2 (referred to as RFP) expressing HeLa cells (obtained from Anticancer) were cultured in

303 RPMI-1640 supplemented with 10% FBS, 2 mM *l*-glutamine (Invitrogen), 1% Penicillin-

304 Streptomycin (Invitrogen). The cells were incubated at 37°C in 5% CO_2 in a humidified

305 incubator.

306

307 **Zebrafish hematogenous metastasis model**

308 Maintenance of the transgenic zebrafish and the experimental design for this study were approved

309   by the Hamamatsu University School of Medicine animal welfare. Zebrafish were maintained

310   according to standard methods [42]. The transgenic strain of zebrafish expressing enhanced green

311   fluorescent protein (EGFP) under the *flk1 (VEGFR2)* promoter (*flk1: EGFP*) was obtained from

312   the Zebrafish International Resource Center [43]. Human cancer cells were microinjected into the

313   zebrafish larvae, following the protocol reported previously with some modifications [7]. Fish

314   larvae were dechorionated and anesthetized with 0.006% tricaine 48 h post-fertilization (hpf;

315   Sigma). Anesthetized larvae were then transferred onto an agarose gel for microinjection. RFP

316   expressing cancer cells were detached from culture dishes using Cell Dissociation Buffer

317   Enzyme-Free PBS-based (13151-014, Gibco) and then were washed twice with PBS. Cancer

318   cells were injected into the common cardinal vein using a tapered borosilicate glass capillary (1.0

319   mm in diameter, World Precision Instruments, Inc.) with a tip diameter of 20 - 40 μm (i.d.)

320   connected to a 50 ml glass syringe. The position of the capillary tip was controlled by a

321   manipulator (M-152, Narishige Scientific). The injected fish larvae were kept at 32˚C in the

322   presence of 25 μg/ml dexamethasone (Sigma) for 5 - 7 h for immunosuppression only before

323   observation because the presence of both tricaine and dexamethasone suppressed the heart beat of

324   larvae. The larvae that formed severe emboli in the arterioles were selected under a fluorescence

325   stereomicroscope (SZX16, Olympus), and used for further experiments.

326

327   **Live imaging of embolus-forming cancer cells and endothelial cells**

328   A small drop of water containing an anesthetized larva was placed in a glass-bottom dish (36 mm,

329   Matsunami, Gifu). One ml of low temperature melting agarose (E-3126-25, BM equipment,

330   Tokyo) containing 0.006% tricaine was added to the dish to hold the larva in a gel attached to the

331   glass at the bottom. The dish was filled with 2 ml water containing 0.006% tricaine. The long

332   time dual color time-lapse recording was carried out by using a homemade imaging system

333   driven by ImageJ software (NIH, USA) or a microscope system in an incubator (BioStation,

334   Nikon, Tokyo). The filter wheels (FW102, Tholabs, NJ) were controlled by the ImageJ software

335   (Research Services Branch, National Institute of Mental Health, Bethesda, Maryland, USA;

336   http://imagej.nih.gov/) through an IJSerial plugin (http://www.eslide.net/ijstage.php) for the dual

337   color fluorescence imaging, and time-lapse images were captured using a QuickTime Capture

338   plugin and Time-Lapse Video macros with some modifications

339   (http://rsbweb.nih.gov/ij/plugins/qt-capture.html). The analog monochrome camera (WAT-

340   120N+, Watec, Tokyo) was connected to the digital converter (ADVC-300, Canopus) and a PC

341   via IEEE1394 interface. The background noise was decreased using an image processor

342   (ARGUS-20, Hamamatsu Photonics, Hamamatsu). The temperature on the stage was maintained

343   at 32˚C using a transparent heating plate (Kitazato, Fuji). In a standard recording, fluorescence

344   images were captured every 5 min for a total time of up to 11 h. The spatial evaluation of cancer

345   cells and endothelial cells was carried out using a confocal microscope (FV1000, Olympus). 3D

346   stack images were taken by confocal microscopy (FV1000, Olympus) and processed using image

347   processing package Fiji (http://fiji.sc/Fiji) [44].

348

349   **RNA interference, RT-qPCR**

350   The siRNA sequence targeting human VEGF-A (referred here as VEGF) was the same as that

351   designed in a previous report [45]: 5'-GGAGUACCCUGAUGAGAUCdTdT-3' (sense), 5'-

352   GAUCUCAUCAGGGUACUCCdTdT-3' (antisense). MISSION siRNA Universal Negative

353   Control (Sigma) was used as a nonsense control siRNA. Relative mRNA amounts were

354   quantified using iQ™ SYBR Green supermix (Bio-Rad Laboratpries, Inc). Forward 5'-

355   CCTGGTGGACATCTTCCAGGAGTA-3' and reverse 5'-

356   CTTGGTGAGGTTTGATCCGCATAA-3' primers were used to detect VEGF, and forward 5'-

357   AACGGATTTGGTCGTATTGGGC-3' and reverse 5'-TTCTCAGCCTTGACGGTGCCAT-3'

358   primers were used to detect glyceraldehyde-3-phosphate dehydrogenase (GAPDH) mRNA. For

359   comparative, quantitative analysis, transcript levels were normalized to the level of GAPDH and

360   changes were determined. The comparative quantitation method ($\Delta\Delta Ct$) was used to compare the

361   different samples and transformed to absolute values with $2^{\wedge}-\Delta\Delta Ct$ for obtaining relative fold

362 changes. All assays were performed in triplicates. VEGF siRNA-treated RFP-HeLa cells were

363 injected into the blood vessels 17 - 19 h after transfection. The cancer cell-injected larvae were

364 kept at 32˚C in the presence of 25 µg/ml dexamethasone for 5 - 7 h for immunosuppression, and

365 these cells were then observed for 11 h within 37 h after the transfection, so that VEGF was

366 efficiently depleted during the observation period.

367

368 **Anti-VEGF treatment**

369 Sunitinib (Toronto Research Chemicals, Toronto), an orally active VEGFR tyrosine kinase

370 inhibitor, was dissolved in dimethyl sulfoxide (DMSO) to make a stock solution of 10 mM. The

371 stock solution was diluted in water to attain a concentration of 5 µM. Sunitinib treatment was

372 started immediately after cancer cell injection. The injected fish larvae were kept at 32˚C in the

373 presence of 25 µg/ml dexamethasone (Sigma) and 5 µM sunitinib for 5 - 7 h for

374 immunosuppression before observation. The cancer cell-injected larvae were then held in glass-

375 bottom dishes with low temperature melting agarose on which water containing 0.006% tricaine

376 and 5 µM sunitinib was added.

377

378 *In vitro* **observation of live cells**

379 The cells were seeded in polymer-bottom dishes (Bio Medical Science, Japan), and time-lapse

380 images were captured every minute for 12 h using BioStation (Nikon).

381

382 **Immunofluorescence**

383 The cells in the polymer-bottom dishes were fixed (4% paraformaldehyde for 15 min),

384 permeabilized (1% Triton X-100 for 15 min) and blocked (PBS containing 2% bovine serum

385 albumin (Sigma, St Louis) for 30 min) for non specific immunostaining. The cells were, then,

386 incubated with anti-vinculin mouse monoclonal antibody (ab18058, 1:200, Abcam, City)

387 overnight at 4˚C, subsequently with anti-mouse-IgG conjugated with Alexa 488 (Invitrogen), and

388   finally with 1 µg/ml Hoechst 33342 (Dojindo, Kamimashiki). The immunostained cells were

389   observed under a confocal microscope (FV1000, Olympus, Hachioji).

390

391   **Chemotactic cell migration assay**

392   The cells were seeded in BD Falcon™ FluoroBlok™ 24-Multiwell Insert Systems (351157, BD,

393   NJ). The bottom wells were filled with chemoattractant-rich NIH3T3 conditioned medium. The

394   cells were stained with calcein-AM (Dojindo) after 24-h incubation, and the number of stained

395   cells in the bottom wells was counted in fluorescence images captured using an inverted

396   fluorescence microscope.

397

398   **Electron microscopy**

399   Fish larvae were fixed for scanning electron microscopy (SEM) by perfusion with 2%

400   paraformaldehyde and 2.5% glutaraldehyde in PBS using the microinjection system for

401   approximately 5 min, and then transferred into the same fixation buffer. Samples were

402   dehydrated in a graded ethanol series, and frozen in liquid nitrogen and cracked into several

403   pieces. These samples were then collected and freeze dried with t-butanol, and stained with OsO_4,

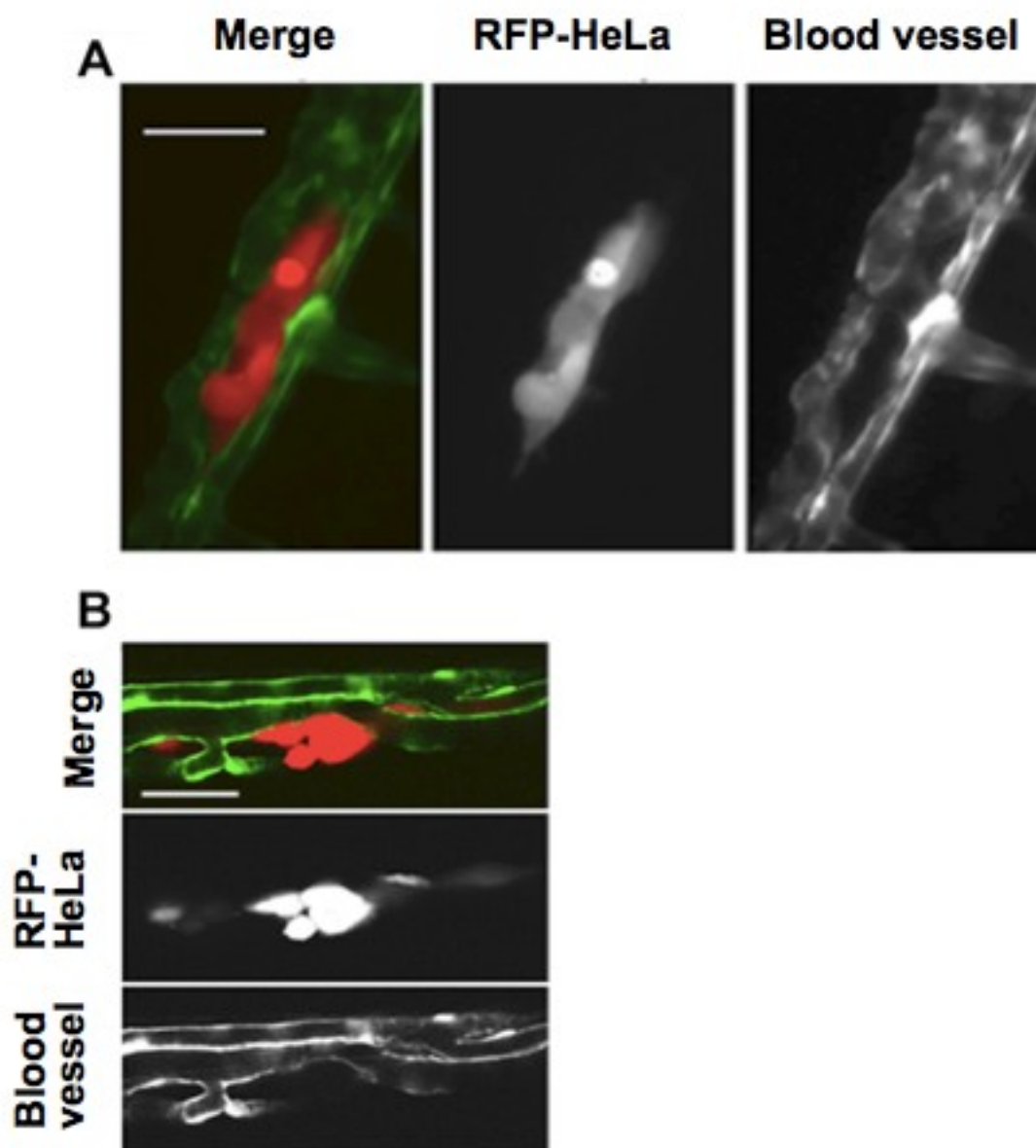404   and examined with a scanning electron microscope (S-4800, Hitachi, Tokyo).

405

Figure 1. Extravasation of Cancer Cells after Severe Emboli Formation in Arterioles of Zebrafish Larvae. A, RFP-HeLa cells and endothelial cells in arterioles were examined under an epifluorescence microscope 17 - 20 h after formation of the emboli. **B**, The spatial locations of the extravasated RFP-HeLa cells and blood vessels were examined under a confocal microscope. Bars, 100 μm (A) or 40 μm (B).
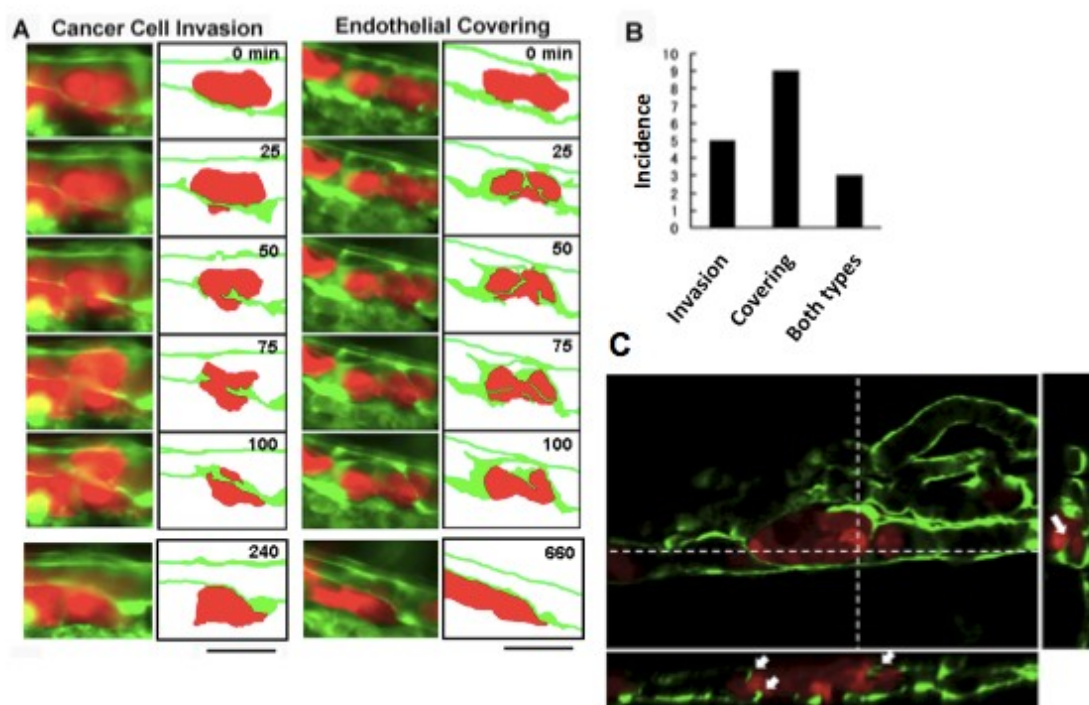
Figure 2. Two Representative processes of Extravasation in Cancer Cells. A, Cancer cell invasion-type and endothelial covering-type extravasation in RFP-HeLa cells. Right panels show schematic outlines of the embolus-forming RFP-HeLa cells (red) and the surrounding endothelial cells (green). The numbers indicate the elapsed time in minutes. Bars, 40 μm. **B**, The incidence of the 2 processes of extravasation. Seven larvae in which RFP-HeLa cells formed severe emboli were observed. Seventeen extravasation events were counted during the 11 h observations. **C**, Side view of 3D reconstructed images. Some endothelial cells were extending over or penetrating through the embolus-forming RFP-HeLa cells (white arrows). Dashed lines in 2D image indicate locations of slicing along a vertical axis.
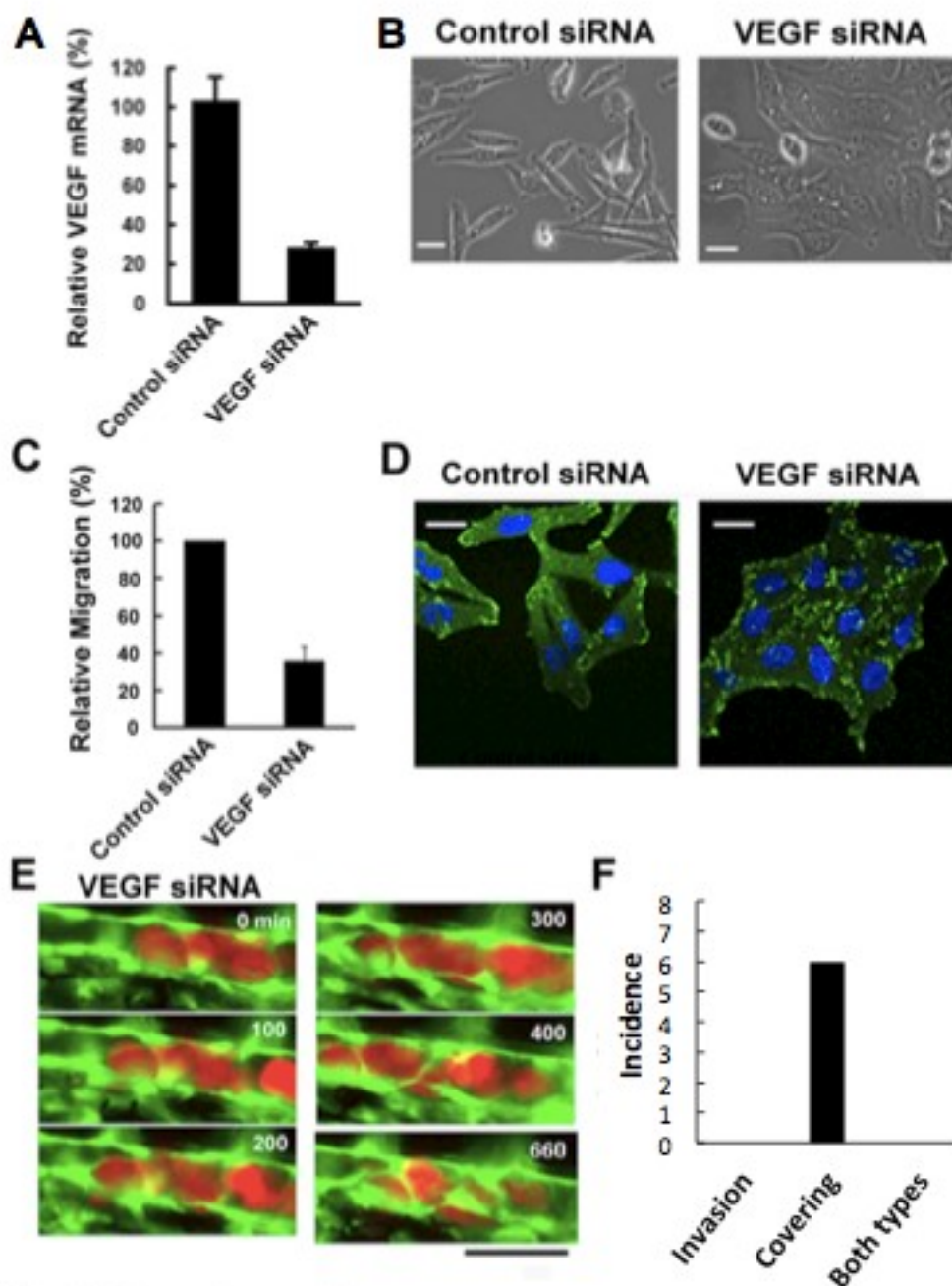
Figure 3. Effects of VEGF Depletion on Cancer Cell Properties and Extravasation. **A**, The

depletion of VEGF in RFP-HeLa cells was confirmed by RT-qPCR 24 h after the transfection

with siRNA. GAPDH was amplified as an internal control. **B**, Phase contrast images of control

siRNA-treated and VEGF-depleted RFP-HeLa cells in culture. **C**, Quantitative evaluation of

chemotactic migration in control siRNA-treated and VEGF-depleted RFP-HeLa cells (mean ±

SD, n = 3). **D**, Confocal microscopic images of control siRNA-treated and VEGF-depleted RFP-

437   HeLa cells showing the distribution of vinculin (green) and DNA (blue). **E**, The extravasation of

438   VEGF-depleted RFP-HeLa cells. The numbers indicate the elapsed time in minutes. **F**, Incidence

439   of the 2 processes of extravasation. Nine larvae in which VEGF-depleted RFP-HeLa cells

440   formed severe emboli were observed. Six extravasation events were counted during 11 h

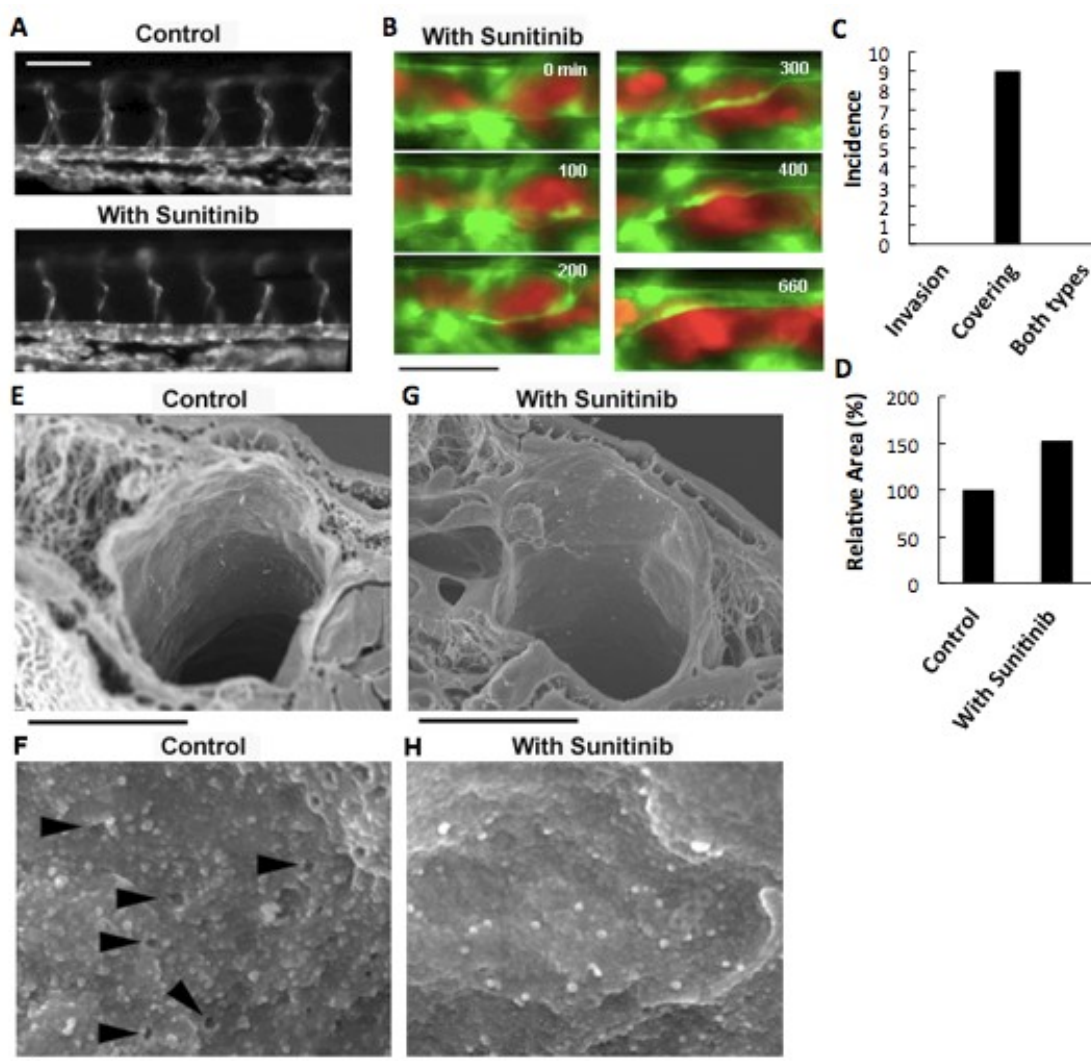441   observations. Bars, 20 μm (B, D) or 40 μm (E).

442

443

444

Figure 4. Effects of Anti-angiogenic Inhibitor, Sunitinib, on the Vasculature of Zebrafish Larvae and Cancer Cell Extravasation. A, Intersegmental vessels were severely deteriorated by treatment with sunitinib. **B**, Extravasation of RFP-HeLa cells in the presence of sunitinib. The numbers indicate the elapsed time in minutes. **C**, The incidence of the 2 processes of extravasation. Seven larvae in which RFP-HeLa cells formed severe emboli were observed in the presence of sunitinib. Nine extravasation events were counted during 11 h observations. **D**, The sum of the area of extravasated cancer cell images was calculated from all of the 7 movies recorded in RFP-HeLa cells with and without sunitinib treatments. Bars, 100 μm (A) or 40 μm (B). **E** and **G**, Scanning electron micrographs of the arteries in the control and sunitinib-treated

454   larvae. Sunitinib-treated larvae showed thicker vascular walls. **F**, The magnified image of the

455   luminal face on the endothelial wall of a control larva. The endothelial wall showed many holes

456   or fenestration-like structures (arrowhead). **H**, The magnified image of the luminal face on the

457   endothelial wall of a sunitinib-treated larva. The endothelial wall showed no fenestration-like

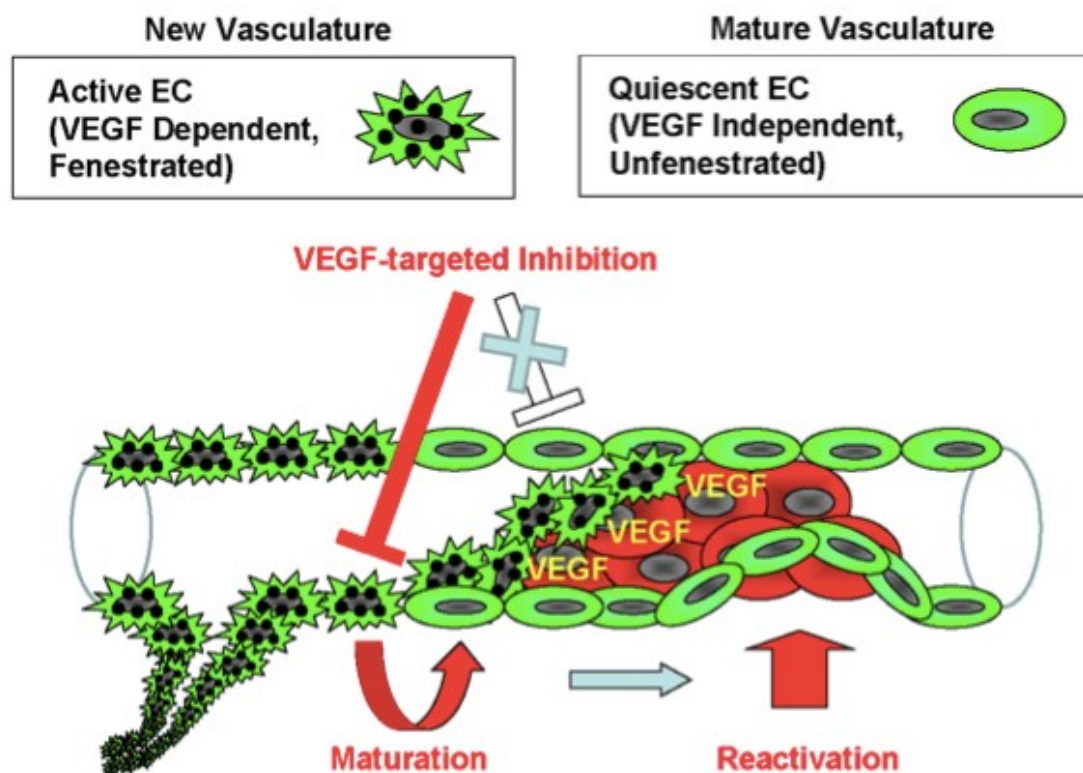458   structures. Bars, 10 μm (E and G) or 0.5 μm (F and H).

459

Figure 5. Model of the endothelial coverage regulation via vascular homeostasis maintenance. Active EC in the normal vasculature, which is VEGF-dependent and fenestrated, and quiescent EC, which is VEGF-independent and unfenestrated, coexist in the same blood vessel. VEGF-targeted inhibitors only affect the active ECs, thus resulting in deterioration of new vasculature via apoptosis or vascular maturation. In contrast, the quiescent ECs that contain mature vasculature are reactivated independently of VEGF in order to maintain vascular homeostasis.

References

1. Gupta GP, Massague J (2006) Cancer metastasis: Building a framework. Cell 127: 679-695.

2. Nguyen DX, Bos PD, Massague J (2009) Metastasis: from dissemination to organ-specific colonization. Nature Reviews Cancer 9: 274-U265.

3. Flusberg BA, Cocker ED, Piyawattanametha W, Jung JC, Cheung ELM, et al. (2005) Fiber-optic fluorescence imaging. Nature Methods 2: 941-950.

4. Beerling E, Ritsma L, Vrisekoop N, Derksen PWB, van Rheenen J (2011) Intravital microscopy: new insights into metastasis of tumors. Journal of Cell Science 124: 299-310.

5. Ritsma L, Steller EJ, Beerling E, Loomans CJ, Zomer A et al., (2012) Intravital microscopy through an abdominal imaging window reveals a pre-micrometastasis stage during liver metastasis. Science Translational Medicine 4: 158ra145.

6. Stoletov K, Montel V, Lester RD, Gonias SL, Klemke R (2007) High-resolution imaging of the dynamic tumor cell-vascular interface in transparent zebrafish. Proceedings of the National Academy of Sciences of the United States of America 104: 17406-17411.

7. Stoletov K, Kato H, Zardouzian E, Kelber J, Yang J, et al. (2010) Visualizing extravasation dynamics of metastatic tumor cells. Journal of Cell Science 123: 2332-2341.

8. Zhang J, Wei J, Kanada M, Yan L, Zhang Z, et al. (2013) Inhibition of store-operated Ca(2+) entry suppresses EGF-induced migration and eliminates extravasation from vasculature in nasopharyngeal carcinoma cell. Cancer Letter 336: 390-397.

9. Berghmans S, Jette C, Langenau D, Hsu K, Stewart R, et al. (2005) Making waves in cancer research: new models in the zebrafish. Biotechniques 39: 227-237.

10. Zon LI, Peterson RT (2005) In vivo drug discovery in the zebrafish. Nature Reviews Drug Discovery 4: 35-44.

11. Stoletov K, Klemke R (2008) Catch of the day: zebrafish as a human cancer model. Oncogene 27: 4509-4520.

12. Lapis K, Paku S, Liotta LA (1988) Endothelialization of embolized tumor cells during metastasis formation. Clinical & experimental metastasis 6: 73-89.

13. Weis S, Cui JH, Barnes L, Cheresh D (2004) Endothelial barrier disruption by VEGF-mediated Src activity potentiates tumor cell extravasation and metastasis. Journal of Cell Biology 167: 223-229.

14. Senger DR, Vandewater L, Brown LF, Nagy JA, Yeo KT, et al. (1993) VASCULAR-PERMEABILITY FACTOR (VPF, VEGF) IN TUMOR BIOLOGY. Cancer and Metastasis Reviews 12: 303-324.

15. Esser S, Lampugnani MG, Corada M, Dejana E, Risau W (1998) Vascular endothelial growth factor induces VE-cadherin tyrosine phosphorylation in endothelial cells. Journal of Cell Science 111: 1853-1865.

16. Bachelder RE, Lipscomb EA, Lin XN, Wendt MA, Chadborn NH, et al. (2003) Competing autocrine pathways involving alternative neuropilin-1 Lligands regulate chemotaxis of carcinoma cells. Cancer Research 63: 5230-5233.

17. Bergers G, Song S, Meyer-Morse N, Bergsland E, Hanahan D (2003) Benefits of targeting both pericytes and endothelial cells in the tumor vasculature with kinase inhibitors. Journal of Clinical Investigation 111: 1287-1295.

18. Pietras K, Hanahan D (2005) A multitargeted, metronomic, and maximum-tolerated dose "chemo-switch" regimen is antiangiogenic, producing objective responses and survival benefit in a mouse model of cancer. Journal of Clinical Oncology 23: 939-952.

19. Gerber HP, Hillan KJ, Ryan AM, Kowalski J, Keller GA, et al. (1999) VEGF is required for growth and survival in neonatal mice. Development 126: 1149-1159.

20. Lee S, Chen TT, Barber CL, Jordan MC, Murdock J, et al. (2007) Autocrine VEGF signaling is required for vascular homeostasis. Cell 130: 691-703.

518 21. Inai T, Mancuso M, Hashizume H, Baffert F, Haskell A, et al. (2004) Inhibition of vascular
519   endothelial growth factor (VEGF) signaling in cancer causes loss of endothelial
520   fenestrations, regression of tumor vessels, and appearance of basement membrane ghosts.
521   American Journal of Pathology 165: 35-52.
522 22. Kamba T, Tam BYY, Hashizume H, Haskell A, Sennino B, et al. (2006) VEGF-dependent
523   plasticity of fenestrated capillaries in the normal adult microvasculature. American
524   Journal of Physiology-Heart and Circulatory Physiology 290: H560-H576.
525 23. Mazzone M, Dettori D, de Oliveira RL, Loges S, Schmidt T, et al. (2009) Heterozygous
526   Deficiency of PHD2 Restores Tumor Oxygenation and Inhibits Metastasis via Endothelial
527   Normalization. Cell 136: 839-851.
528 24. Middleton J, Patterson AM, Gardner L, Schmutz C, Ashton BA (2002) Leukocyte
529   extravasation: chemokine transport and presentation by the endothelium. Blood 100:
530   3853-3860.
531 25. Ebos JML, Lee CR, Cruz-Munoz W, Bjarnason GA, Christensen JG, et al. (2009) Accelerated
532   Metastasis after Short-Term Treatment with a Potent Inhibitor of Tumor Angiogenesis.
533   Cancer Cell 15: 232-239.
534 26. Paez-Ribes M, Allen E, Hudock J, Takeda T, Okuyama H, et al. (2009) Antiangiogenic
535   Therapy Elicits Malignant Progression of Tumors to Increased Local Invasion and Distant
536   Metastasis. Cancer Cell 15: 220-231.
537 27. Loges S, Mazzone M, Hohensinner P, Carmeliet P (2009) Silencing or Fueling Metastasis
538   with VEGF Inhibitors: Antiangiogenesis Revisited. Cancer Cell 15: 167-170.
539 28. Brahimi-Horn MC, Chiche J, Pouyssegur J (2007) Hypoxia and cancer. Journal of Molecular
540   Medicine-Jmm 85: 1301-1307.
541 29. Semenza GL (2003) Targeting HIF-1 for cancer therapy. Nature Reviews Cancer 3: 721-732.
542 30. Phng LK, Gerhardt H (2009) Angiogenesis: A Team Effort Coordinated by Notch.
543   Developmental Cell 16: 196-208.
544 31. Willett CG, Boucher Y, Duda DG, di Tomaso E, Munn LL, et al. (2005) Surrogate markers for
545   antiangiogenic therapy and dose-limiting toxicities for bevacizumab with radiation and
546   chemotherapy: Continued experience of a phase I trial in rectal cancer patients. Journal of
547   Clinical Oncology 23: 8136-8139.
548 32. Ebos JML, Lee CR, Christensen JG, Mutsaers AJ, Kerbel RS (2007) Multiple circulating
549   proangiogenic factors induced by sunitinib malate are tumor-independent and correlate
550   with antitumor efficacy. Proceedings of the National Academy of Sciences of the United
551   States of America 104: 17069-17074.
552 33. Casanovas O, Hicklin DJ, Bergers G, Hanahan D (2005) Drug resistance by evasion of
553   antiangiogenic targeting of VEGF signaling in late-stage pancreatic islet tumors. Cancer
554   Cell 8: 299-309.
555 34. Hurwitz H, Fehrenbacher L, Novotny W, Cartwright T, Hainsworth J, et al. (2004)
556   Bevacizumab plus irinotecan, fluorouracil, and leucovorin for metastatic colorectal
557   cancer. New England Journal of Medicine 350: 2335-2342.
558 35. Miller K, Wang ML, Gralow J, Dickler M, Cobleigh M, et al. (2007) Paclitaxel plus
559   bevacizumab versus paclitaxel alone for metastatic breast cancer. New England Journal of
560   Medicine 357: 2666-2676.
561 36. Demetri GD, van Oosterom AT, Garrett CR, Blackstein ME, Shah MH, et al. (2006) Efficacy
562   and safety of sunitinib in patients with advanced gastrointestinal stromal tumour after
563   failure of imatinib: a randomised controlled trial. Lancet 368: 1329-1338.
564 37. Motzer RJ, Michaelson MD, Redman BG, Hudes GR, Wilding G, et al. (2006) Activity of
565   SU11248, a multitargeted inhibitor of vascular endothelial growth factor receptor and
566   platelet-derived growth factor receptor, in patients with metastatic renal cell carcinoma.

567   Journal of Clinical Oncology 24: 16-24.

568   38. Abou-Alfa GK, Schwartz L, Ricci S, Amadori D, Santoro A, et al. (2006) Phase II study of
569   sorafenib in patients with advanced hepatocellular carcinoma. Journal of Clinical
570   Oncology 24: 4293-4300.

571   39. Escudier B (2007) Sorafenib in advanced clear-cell renal-cell carcinoma (vol 356, pg 125,
572   2007). New England Journal of Medicine 357: 203-203.

573   40. Grepin R, Pages G (2010) Molecular mechanisms of resistance to tumour anti-angiogenic
574   strategies. Journal of oncology 2010: 835680.

575   41. Kerbel RS (2008) Molecular origins of cancer: Tumor angiogenesis. New England Journal of
576   Medicine 358: 2039-2049.

577   42. Westerfield M (1993) The Zebrafish Book. Univ. Oregon Press, Eugene, Oregon.

578   43. Jin S-W, Beis D, Mitchell T, Chen J-N, Stainier DYR (2005) Cellular and molecular analyses
579   of vascular tube and lumen formation in zebrafish. Development (Cambridge, England)
580   132: 5199-5209.

581   44. Schindelin J, Arganda-Carreras I, Frise E, Kaynig V, Longair M, et al. (2012) Fiji: an open-
582   source platform for biological-image analysis, Nature Methods 9: 676-682.

583   45. Takei Y, Kadomatsu K, Yuzawa Y, Matsuo S, Muramatsu T (2004) A small interfering RNA
584   targeting vascular endothelial growth factor as cancer therapeutics. Cancer Research 64:
585   3365-3370.

586

587